Construction and Modeling of a Variable Collective Pitch Coaxial UAV

Jinqiang Cui[1], Fei Wang[1], Zhengyin Qian[2], Ben M. Chen[2] and Tong H. Lee[2]

[1]*NUS Graduate School for Integrative Sciences & Engineering, National University of Singapore, Singapore, Singapore*
[2]*Department of Electrical & Computer Engineering, National University of Singapore, Singapore, Singapore*

Keywords: Coaxial Helicopter, Unmanned Aerial Vehicle, Flapping Dynamics, Model Identification.

Abstract: This paper describes the construction and modeling of a coaxial unmanned aerial vehicle for in-forest operation. The bare helicopter platform is upgraded and mounted with an onboard navigation system, which includes central processing units and sensors such as inertial measurement unit, camera and scanning laser range finder. The model structure of the helicopter is formulated, in which the model of rotor thrust and roll-pitch dynamics are described in details. The flapping dynamics of the rotor and the stabilizer bar are presented and lumped into a state-space model. The parameters of the state-space model are identified in frequency domain using CIFER. Time domain verification with a new set of flight data exhibits excellent agreement with the prediction of the identified model.

1 INTRODUCTION

With the rapid development of unmanned aerial vehicles (UAVs), a wide range of platforms have been developed. Model-scale helicopter is one of the more popular type due to its vertical take-off and landing capability. A single rotor UAV based on Yamaha *R-50* with a rotor diameter of 3.07 m has been developed by Carnegie Mellon Univerisity (Mettler et al., 1999; Mettler, 2002) and the linear UAV models for hover and cruise flight have been identified. A comprehensive nonlinear model for a similar small-scale single-rotor UAV has been presented by researchers in National University of Singapore (Cai et al., 2012). A micro coaxial indoor UAV (muFly) with a rotor diameter of 0.34 m has been modeled and identified by researchers in ETH Zürich (Schafroth et al., 2010). Now muFly is commercially available from Skybotix (CoaX), which can be an ideal platform for indoor operation and advanced controller design (Fankhauser et al., 2011).

In our research scope, we intend to develop a UAV that is capable of flying through the forest. Thus the platform has to be compact enough to fly among tree trunks. Compared to single rotor helicopters, coaxial helicopters produce better lift efficiency by avoiding power losses from the tangential airflow. What's more, coaxial helicopter is also inherently more stable than single rotor helicopters. Therefore, we choose a coaxial helicopter as the main frame of our UAV platform.

In this paper, we first describe the mechanical structure of the coaxial helicopter and the onboard navigation system in section 2. In section 3, we first present the model structure of the coaxial helicopter, then we derive the dual rotor thrust empirically based on the near-hover flight assumption. The flapping dynamics of the rotor and stabilizer bar are presented separately before they are lumped into a state-space model. Following this, the lumped system is identified in frequency domain and verified in time domain. Section 4 concludes the paper.

2 PLATFORM DEVELOPMENT

2.1 Bare Helicopter

The 'Kaa-350' is a coaxial helicopter made in Germany according to the design of full scale coaxial helicopter from the Kamov design bureau. This helicopter has a rotor diameter of 0.7 m and weighs 990 g without battery. Its rotor head is equipped with integrated hinges and shock resistant dampers. With the recommended configuration of motor, electronic speed controller (ESC) and blades, it can fly safely with a total weight of 2.3 kg. The mechanical structure of 'Kaa-350' is shown in Fig. 1. The rotor blades are not assembled in order to better illustrate the struc-
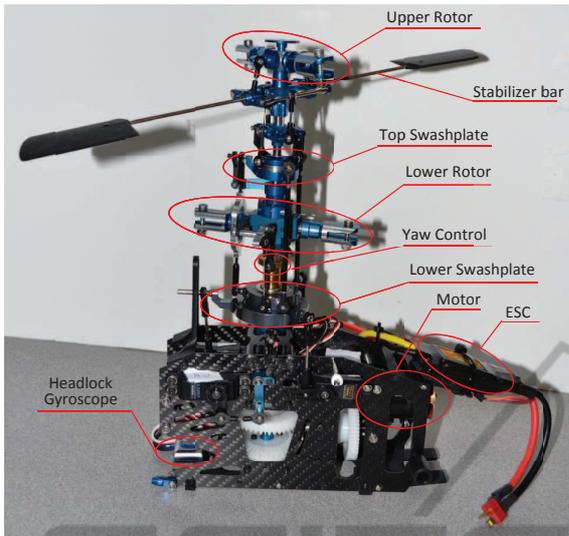
Figure 1: Description of bare helicopter.

ture. The helicopter consists of two contrarotating rotors: the upper rotor and the lower rotor. The pitch angles of the two rotors are controlled by the top swashplate and the lower swashplate respectively. The two swashplates are always parallel to each other since they are connected by three linkages which rotate with the top swashplate. The upper rotor is equipped with a stabilizer bar through a Bell-Hiller mixer which also influences the cyclic pitch of the upper rotor blade. The upper rotor and lower rotor are driven by the same brushless DC electric motor powered by a 3-cell lithium-polymer battery through the ESC. The rotation speed of the upper rotor and the lower rotor are thus always the same. Collective and cyclic inputs from servos are transferred to the lower swashplate and top swashplate simultaneously, resulting in dynamic movement of the helicopter in heave direction or pitch-roll direction. The yaw direction control is realized by changing the collective pitch of the lower rotor.

2.2 Onboard System

The helicopter gains autonomous capability provided that it is equipped with an onboard navigation system. This system consists of various sensors and signal processing units. As shown in Fig. 2, the avionic system includes sensors such as inertial measurement unit (IMU), magnetometer, GPS, scanning laser range finder and camera. The central processing units are two gumstix (Overo Fire) units. One gumstix implements the autonomous control of the helicopter while the other gumstix is responsible for processing image sequences captured by the camera. Serial com-
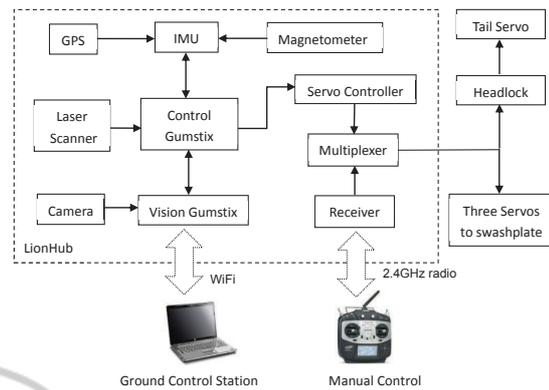

Figure 2: Avionic System Configuration.

munication is established between the two gumstix units. The control gumstix also reads the outputs of onboard sensors and generates autonomous control signals which are passed to the servo controller and fed into the multiplexer. The multiplexer has two 4-channel input ports and one 4-channel output port. Manual control signals from the pilot are transmitted to the receiver via 2.4 GHz radio and fed into the multiplexer. The outputs of multiplexer are connected to the three servos controlling the swashplates and the headlock gyro mixer. The headlock gyro mixer mixes the yaw control signal and the output of the headlock gyroscope to generate a composite yaw control signal that controls the yaw servo. The multiplexer is indispensable since the helicopter may encounter unexpected situations during flight where an instant switch to manual control is required to save the helicopter. During manual flight or autonomous flight, helicopter states and sensor outputs are logged online and critical information are transferred to ground station via WiFi communication. Control command from ground station could also be transmitted to the helicopter in autonomous flight mode. Fig. 3 shows the completed UAV platform operating in the air.

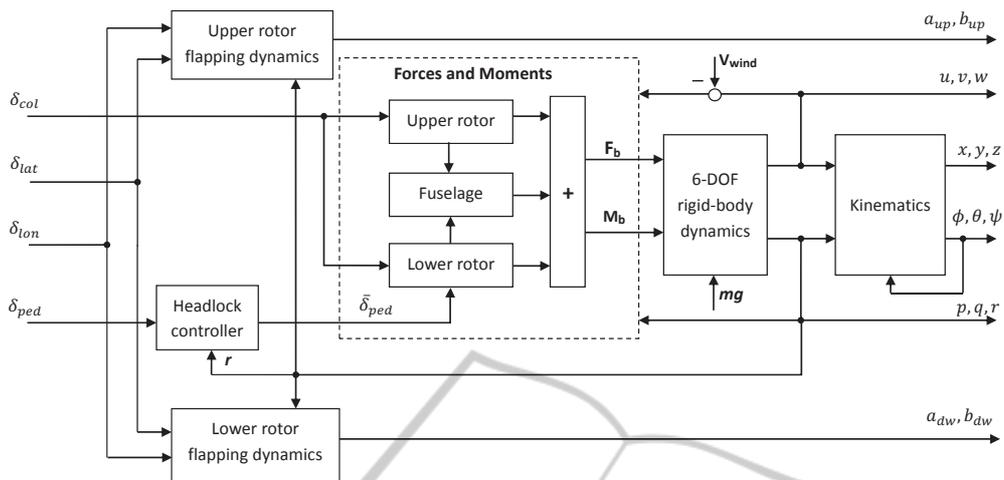Figure 3: Helicopter flying in the air.

Figure 4: Model Structure Overview.

3 MODELING AND PARAMETER IDENTIFICATION

3.1 Model Structure

The UAV model structure is shown in Fig. 4. The collective input δ_{col} controls the collective pitch angles of both upper and lower rotors through the two parallel swashplates. The cyclic inputs δ_{lat} and δ_{lon} tilt the upper and lower swashplates and generate flapping motion for both rotors, causing the longitudinal and lateral movements of the helicopter. The yaw channel control δ_{ped} is first mixed with the output of the headlock gyro (PI controller) before it is applied on the collective pitch of the lower rotor. The model is denoted in a compact form as follows,

$$\dot{\mathbf{x}} = \mathbf{f}(\mathbf{x}, \mathbf{u}, \mathbf{w}) , \qquad (1)$$

where

$$\mathbf{x} = (x \quad y \quad z \quad u \quad v \quad w \quad \phi \quad \theta \quad \psi \cdots$$
$$\cdots p \quad q \quad r \quad a_{up} \quad b_{up} \quad a_{dw} \quad b_{dw} \quad r_f)^{\mathrm{T}} ,$$
$$\mathbf{u} = (\delta_{lat} \quad \delta_{lon} \quad \delta_{col} \quad \delta_{ped})^{\mathrm{T}} ,$$
$$\mathbf{w} = (\omega_u \quad \omega_v \quad \omega_w)^{\mathrm{T}} .$$

$\mathbf{x}$ is the state vector, $\mathbf{u}$ is the input vector, δ_{col}, δ_{lat}, δ_{lon} and δ_{ped} are the collective, lateral, longitudinal and pedal inputs to the whole system. $\mathbf{w}_w$ stands for the wind disturbance velocity. The overall dynamics of the helicopter could be separated into three subsystems: the roll-pitch dynamics, the yaw dynamics and the heave dynamics. The roll-pitch dynamics, capturing the angular responses of helicopter to the cyclic inputs, constitutes the core of helicopter dynamics (Mettler et al., 1999). Thus we mainly present our results in the modeling and identification of the roll-pitch dynamics in this paper.

3.2 Thrust Formulation

It is a very complex issue to address the coaxial rotor aerodynamics. A comprehensive survey (Coleman, 1997) has covered the major aerodynamic experiments and computational models dealing with coaxial rotor systems. It covered issues of separation distance, load sharing between rotors, wake structure, solidity effects, swirl recovery, and the effects of having no tail rotor. (Lim et al., 2009) investigated the ground and rotor spacing effects and Reynolds number scaling effect by comparing three rotor configurations, concluding that the coaxial rotor spacing effect on hover performance was minimal for the rotor spacing larger than 20% of the rotor diameter. Researchers (Kim and Brown, 2008; Kim and Brown, 2006) at Glasgow University has developed a Vorticity Transport Model (VTM) to study the aerodynamics of coaxial rotor systems. They stated that the state-of-the-art computational modeling of helicopter aerodynamics had managed to model the interactive aerodynamic flow field associated with a coaxial rotor system.

Since the designed UAV will work at near-hover condition, we decide to first extract an empirical relationship between dual rotor thrust T_{mr} and collective input δ_{col}. A test bench is utilized to facilitate a series of tests where the dual rotor thrust and collective input are recorded simultaneously. Fig. 5 shows the results of five tests performed on two fully charged batteries. After fitting the results using the least square method and averaging the five groups of coefficients, a linear
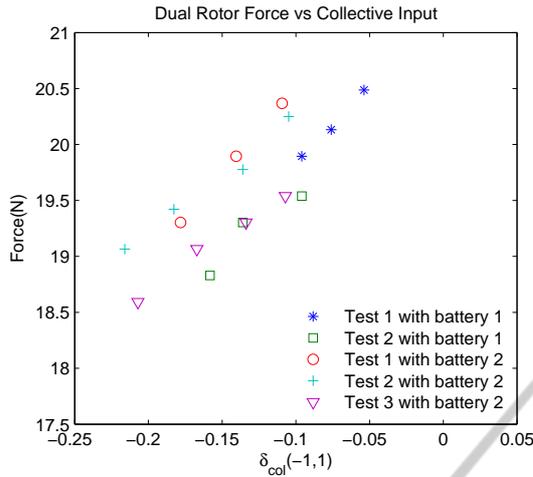
Figure 5: Thrust of dual rotor against collective input.

relationship is obtained as:

$$T_{mr} = K_t \delta_{col} + T_0 , \qquad (2)$$

where $K_t = 10.09\,\text{N}$ and $T_0 = 20.812\,\text{N}$.

For near-hover flight, the direction of the rotor thrust can be assumed to remain perpendicular to the rotor tip-path-plane. The projections of main rotor thrust on the helicopter body axes are defined as:

$$X_{mr} = -T_{mr} \sin a_s , \qquad (3)$$
$$Y_{mr} = T_{mr} \sin b_s , \qquad (4)$$
$$Z_{mr} = -T_{mr} \cos a_s \cos b_s . \qquad (5)$$

The moments generated by the main rotor are:

$$L_{mr} = (K_\beta + T_{mr} H_{mr}) \sin(b_s), \qquad (6)$$
$$M_{mr} = (K_\beta + T_{mr} H_{mr}) \sin(a_s), \qquad (7)$$

where K_β is the spring constant, H_{mr} is the distance from center of gravity (CG) to the middle of two rotor planes, a_s and b_s are the equivalent longitudinal and lateral flapping angles respectively. The torques from upper rotor and lower rotor are balanced when no heading change is required.

3.3 Flapping Dynamics

3.3.1 Bare Rotor Flapping Dynamics

One way to represent the rotor dynamics is to regard it as a rigid disc which can tilt about the longitudinal and lateral axes. Detail description of the rotor equations are extremely complicated. Here, a simplified formulation is adopted, where the rotor forces and moments are expressed as a polynomial function of the rotor state variables (Mettler, 2002). Moreover,

by removing the higher order terms of the Tip-Path-Plane (TPP) equation, the remaining first-order rotor dynamics could be expressed as:

$$\tau_r \dot{b}_i = -b_i - \tau_r p + B_a a_i + \theta_{cyc,bi} , \qquad (8)$$
$$\tau_r \dot{a}_i = -a_i - \tau_r q + A_b b_i + \theta_{cyc,ai} , \qquad (9)$$

where

$$A_b = -B_a = \frac{8K_\beta}{\gamma_{dw} \Omega_{mr}^2 I_{\beta,mr}} , \qquad (10)$$

$$\tau_r = \frac{16}{\gamma_r \Omega_{mr}} \left(1 - \frac{8e_{mr}}{3R_{mr}} \right)^{-1} , \qquad (11)$$

$$\gamma_r = \frac{\rho c_{mr} C_{l\alpha,mr} R_{mr}^4}{I_{\beta,mr}} . \qquad (12)$$

a_i and b_i (i represents $\{up, dw\}$) are the first-order TPP flapping angles in the longitudinal and lateral directions for upper and lower rotors. τ_r and γ_r are the flapping time constant and the lock number of the rotor blades respectively, $I_{\beta,mr}$ is the blade moment of inertia. $\theta_{cyc,a}$ and $\theta_{cyc,b}$ are the longitudinal and lateral cyclic pitch of rotor blade. The approximate formulation in Eq.(8-9) characterizes the crucial TPP responses with respect to cyclic control inputs and helicopter motion.

3.3.2 Stabilizer Bar Flapping Dynamics

The stabilizer bar, which is attached to the upper main rotor shaft via a free-teetering hinge, can be regarded as a secondary rotor. It consists of two paddles and a steel rod. The stabilizer bar is not designed to produce thrust or moment on the main hub, whereas its main function is to adjust the helicopter dynamics via the Bell-Hiller mixer by augmenting the cyclic pitch command of the upper rotor. It serves as a feedback system which increases the helicopter robustness against wind gust and turbulence (Cai et al., 2011). The flapping dynamics of stabilizer bar can be expressed as two first-order differential equations:

$$\dot{c}_s = -q - \frac{1}{\tau_{sb}} c_s + \frac{C_{lon}}{\tau_{sb}} \delta_{lon} , \qquad (13)$$

$$\dot{d}_s = -p - \frac{1}{\tau_{sb}} d_s + \frac{D_{lat}}{\tau_{sb}} \delta_{lat} , \qquad (14)$$

where τ_{sb} is the stabilizer bar flapping time constant, and it can be calculated as

$$\tau_{sb} = \frac{16}{\gamma_{sb} \Omega_{mr}} , \qquad (15)$$

where γ_{sb} is the stabilizer bar Lock number:

$$\gamma_{sb} = \frac{\rho c_{sb} C_{l\alpha,sb} \left(R_{sb}^4 - r_{sb}^4 \right)}{I_{\beta,sb}} . \qquad (16)$$

The free-teetering hinge does not constrain the flapping of stabilizer bar, thus there is no coupling between the longitudinal and lateral flapping motions. The augmented rotor cyclic pitch of upper rotor can be expressed as

$$\theta_{cyc,aup} = A_{lon}\delta_{lon} + K_{sb}c_s , \qquad (17)$$
$$\theta_{cyc,bup} = B_{lat}\delta_{lat} + K_{sb}d_s , \qquad (18)$$

where K_{sb} is the ratio of rotor blade cyclic pitch to stabilizer bar flapping.

3.3.3 Lumped Flapping Dynamics

In this coaxial helicopter configuration, the upper rotor and the lower rotor receive the same cyclic input (δ_{lon}, δ_{lat}) since the top swashplate and bottom swashplate are always parallel. To minimize the overall complexity of the model, the two counter rotating rotor discs are treated as one equivalent rotor disc with respect to flapping motions. Thus there exists only two equivalent flapping angles (a_s, b_s). This assumption produces accurate results which are shown in section 3.3.4. Combining Eq. 8-18, the lumped flapping dynamics subsystem could be represented in the following state space model:

$$\dot{\mathbf{x}} = \mathbf{A}\,\mathbf{x} + \mathbf{B}\,\mathbf{u} , \qquad (19)$$
$$\dot{\mathbf{y}} = \mathbf{C}\,\mathbf{x} , \qquad (20)$$

where

$$\mathbf{A} = \begin{bmatrix} 0 & 0 & 0 & L_b \\ 0 & 0 & M_a & 0 \\ 0 & -1 & -\dfrac{1}{\tau} & \dfrac{A_b}{\tau} \\ -1 & 0 & \dfrac{B_a}{\tau} & -\dfrac{1}{\tau} \end{bmatrix} , \qquad (21)$$

$$\mathbf{B} = \begin{bmatrix} 0 & 0 \\ 0 & 0 \\ 0 & A'_{lon} \\ B'_{lat} & 0 \end{bmatrix} , \qquad (22)$$

$$\mathbf{C} = \begin{bmatrix} 1 & 0 & 0 & 0 \\ 0 & 1 & 0 & 0 \end{bmatrix} , \qquad (23)$$

$$\mathbf{x} = \begin{bmatrix} p \\ q \\ a_s \\ b_s \end{bmatrix} , \quad \mathbf{u} = \begin{bmatrix} \delta_{lat}(t - \tau_{lat}) \\ \delta_{lon}(t - \tau_{lon}) \end{bmatrix} , \quad \mathbf{y} = \begin{bmatrix} p \\ q \end{bmatrix} , \quad (24)$$

$$L_b = \frac{mgH_{mr} + K_\beta}{J_{xx}} , \quad M_a = \frac{mgH_{mr} + K_\beta}{J_{yy}} . \qquad (25)$$

The rotor spring constant K_β, the lateral and longitudinal control derivatives B'_{lat}, A'_{lon}, the lateral and longitudinal control delay τ_{lat}, τ_{lon}, and the equivalent flapping time constant τ are to be identified via frequency domain identification in section 3.3.4. The coupling term A_b and B_a are neglected.

3.3.4 Roll-Pitch Dynamics Identification

The flapping dynamics identification makes full use of a toolkit called CIFER developed by the U.S. Army and NASA specifically for rotorcraft applications (Mettler et al., 1999). It incorporates a range of utilities to support the various steps of the identification process. Flight tests featuring frequency-sweep input in the longitudinal and lateral directions are performed multiple times. During the flights, the control inputs and the helicopter angular rates are recorded online with a sampling rate of 50 Hz. CIFER identifies the model parameters by searching for the best-fit parameters to match frequency responses between the flight test data and the hypothetic model. Fig. 6 shows the on-axis pitch angular rate response with respect to longitudinal input. The coherence level remains above 0.6 up to 30 rad/s. This good coherence indicates the good linearity of the helicopter in hover flight (Tischler and Remple, 2006). Time domain verification is also performed with another flight test data which is not used in the identification process. Fig.7 shows excellent agreement between the model simulation and the flight data in both longitudinal direction. The same process is applied to the lateral direction where the roll dynamics is identified in frequency domain and verified in time domain. Table. 1 lists the values of the identified parameters together with their Cramer-Rao percent and insensitivity. The Cramer-Rao percent and insensitivity are less than 15% and 5% respectively, indicating the high accuracy of the identified parameter.
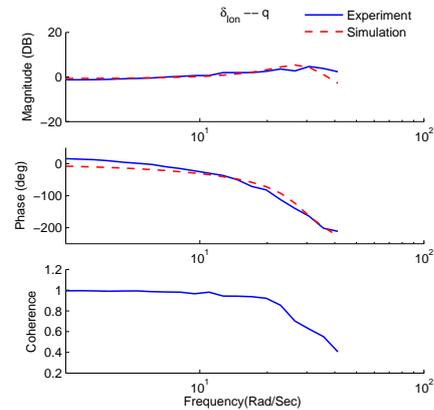

Figure 6: Comparison of frequency response from longitudinal input to pitch angular rate.

4 CONCLUSIONS AND FUTURE WORK

In this paper we have presented our current progress

Table 1: Parameters identified from CIFER.

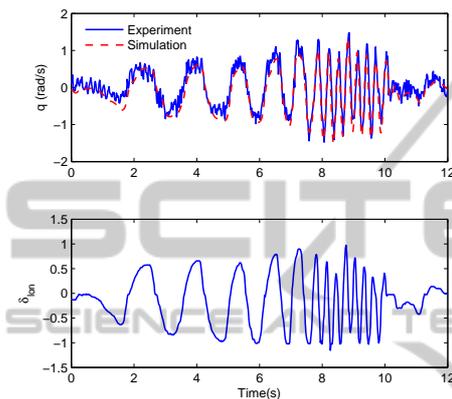| Parameter	Cramer-Rao Percent(%)	Insensitivity(%)	Physical meaning
$L_b = 675.8\,\mathrm{s}^{-2}$	7.171	2.433	Lateral rotor spring derivative
$M_a = 794.7\,\mathrm{s}^{-2}$	7.525	2.589	Longitudinal rotor spring derivative
$\tau = 0.068\,\mathrm{s}$	9.301	3.537	Equivalent flapping time constant
$A'_{lon} = 0.898\,\mathrm{rad/s}$	4.152	1.962	Longitudinal control derivative
$B'_{lat} = 1.069\,\mathrm{rad/s}$	4.157	1.935	Lateral control derivative
$\tau_{lat} = 0.03355\,\mathrm{s}$	12.08	4.477	Lateral control delay
$\tau_{lon} = 0.03390\,\mathrm{s}$	12.17	4.440	Longitudinal control delay
$K_\beta = 11.5029\,\mathrm{Nm}$	NA	NA	Rotor spring constant

Figure 7: Time domain verification of longitudinal input to pitch angular rate.

regarding the development and modeling of a coaxial UAV platform. For platform construction, the payload capability of the bare coaxial helicopter is guaranteed by careful selection of the key components such as motor, blade and ESC. The onboard avionic system is designed and assembled onto the helicopter frame using mechanical dampers. For modeling of the helicopter, the model structure of the platform has been laid out. The coaxial rotor thrust has been empirically derived. More importantly, the roll-pitch dynamics of the helicopter are formulated. Through frequency domain identification in CIFER, the equivalent flapping time constant and spring constant are fine-tuned. Time domain verification using a new set of test data has validated the fidelity of the identified roll-pitch dynamics. Future research work will focus on the modeling of heave dynamics and yaw dynamics which will produce a complete model. Additional effort will be made to study the coaxial rotor wake structure so that an optimal coaxial configuration could be achieved.

ACKNOWLEDGEMENTS

REFERENCES

Cai, G., Chen, B. M., and Lee, T. H. (2011). *Unmanned Rotorcraft Systems*. Springer, London.

Cai, G., Chen, B. M., Lee, T. H., and Lum, K.-Y. (2012). Comprehensive nonlinear modeling of a miniature unmanned helicopter. *Journal of the American Helicopter Society*, 57(1):1–13.

Coleman, C. P. (1997). A survey of theoretical and experimental coaxial rotor aerodynamic research. Technical report, NASA Ames Research Center.

Fankhauser, P., Bouabdallah, S., Leutenegger, S., and Siegwart, R. (2011). Modeling and decoupling control of the coax micro helicopter. In *Proc. of the IEEE/RSJ International Conference on Intelligent Robots and Systems (IROS)*.

Kim, H. and Brown, R. (2006). Coaxial rotor performance and wake dynamics in steady and manoeuvring flight. In *American Helicopter Society 62nd Annual Forum Proceedings*, volume 62, page 20.

Kim, H. and Brown, R. (2008). Modelling the aerodynamics of coaxial helicopters–from an isolated rotor to a complete aircraft. In *Proceedings of the EU-Korea Conference on Science and Technology*, pages 45–59.

Lim, J. W., McAlister, K. W., and Johnson, W. (2009). Hover performance correlation for full-scale and model-scale coaxial rotors. *Journal of the American Helicopter Society*.

Mettler, B. (2002). *Identification Modeling and Characteristics of Miniature Rotorcraft*. Kluwer Academic Publisher, Nowell, MA.

Mettler, B., Tischler, M. B., and Kanade, T. (1999). System identification of small-size unmanned helicopter dynamics. In *American Helicopter Society 55th Annual Forum Proceedings*, volume 2, pages 1706–1717.

Schafroth, D., Bermes, C., Bouabdallah, S., and Siegwart, R. (2010). Modeling and system identification of the mufly micro helicopter. *Journal of intelligent & robotic systems*, 57(1):27–47.

Tischler, M. and Remple, R. (2006). *Aircraft and rotorcraft system identification: Engineering Methods with Flight Test Examples*. AIAA.